Journal of Alloys and Compounds 509 (2011) 3314–3318

Contents lists available at ScienceDirect

Journal of Alloys and Compounds

journal homepage: www.elsevier.com/locate/jallcom

Fe:ZnSe semiconductor nanocrystals: Synthesis, surface capping, and optical properties

Ruishi Xie, Lihua Li, Yuanli Li, Lingyun Liu, Dingquan Xiao, Jianguo Zhu*

College of Materials Science and Engineering, Sichuan University, No. 29, Wangjiang Road, Chengdu 610064, China

ARTICLE INFO

Article history:
Received 23 September 2010
Received in revised form 5 December 2010
Accepted 7 December 2010
Available online 14 December 2010

Keywords:
Chemical synthesis
Nanostructured materials
Doping
Optical properties

ABSTRACT

Water-soluble Fe-doped ZnSe (Fe:ZnSe) nanocrystals (NCs) were synthesized by aqueous synthesis approach using thioglycolic acid (TGA) as capping agent. The undoped ZnSe and Fe:ZnSe NCs were well retained in the zinc blende structure, and the Fe dopants were well doped into the ZnSe NCs, as confirmed by X-ray photoelectron spectroscopy (XPS). The lattice constant of Fe:ZnSe NCs decreases slightly by the introduction of Fe, and Fe:ZnSe NCs exhibit a uniform size distribution with average grain size of ~5 nm. The thioglycolic acid (TGA) was successfully capped on the surface of Fe:ZnSe NCs, confirmed by Fourier-transform-infrared (FT-IR) spectroscopy. The absorption edges of pure ZnSe and Fe:ZnSe NCs are blue-shifted compared to that of corresponding bulk ZnSe, indicating the quantum confinement effect, and the absorption edge of Fe:ZnSe NCs shows a slightly red shift with respect to the pure ZnSe NCs. The as-prepared Fe:ZnSe NCs exhibits an emission peak at ~425 nm, and the photoluminescence (PL) intensity of the NCs has the maximum value when the Fe-doping concentration reaches 1.0 at%. It is of interest to note that the concentration quenching effect appears when the Fe-doping concentration is larger than 10.0 at%, and the underlying physical mechanisms were discussed.

1. Introduction

Colloidal semiconductor nanocrystals (NCs) have currently been attracting widespread scientific and technological interest due to their unique size-tunable optical and electronic properties as well as their potential applications in solar cells, light-emitting diodes (LEDs) and bio-labels [1–12], etc. However, the small ensemble stokes shifts of intrinsic NCs emitters make self-quenching, that is a serious issue if the fluorescent labels must either be kept close to, or be in, a high absorbance [13]. Recently, a new class of potential fluorescence emitter-doped NCs, which are based on transition-metal-ion (Mn, Co, Cu, etc.) doped NCs without heavy-metal ions, can overcome the problems of traditional NCs mentioned above [13,14]. Wide-band-gap II–VI semiconductor NCs have recently attracted considerable attention as a new generation of luminescent NCs, such as ZnS and ZnSe doped with transition-metal ions [13–15].

Zinc selenide (ZnSe), as a wide band gap (2.69 eV) group II–VI semiconductor with large binding energy and a small exciton Bohr radius of 3.8 nm at room temperature [16,17], has some promising applications in light-emitting diodes (LEDs) [18], photodetectors [19], blue-green lasers [20], and window materials in the field of photovoltaics [18]. ZnSe nanostructures in the form of nanorings [18], nanowires [19], nanoribbons [21], and nanotubes [20], have been synthesized. A large number of high-quality transition-metal-ion doped ZnSe NCs, such as Co:ZnSe [14,22], Cu:ZnSe [23–26] and Mn:ZnSe [27–29], have also been successfully prepared through organometallic route. However, this route is not cost-effective because of expensive processing conditions (inert atmosphere and elevated temperature above 300 °C), and as-prepared NCs are hydro-phobic and cannot be used directly for biological and other applications, whereas water-soluble NCs are essential. As compared with the organometallic route, the cheaper, simpler and less toxic aqueous synthesis approach is an alternative strategy to directly prepare water-soluble NCs, and the NCs synthesized in aqueous solution are biologically compatible and more suitable for these biomedical applications. Furthermore, as compared with the other existing techniques (coprecipitation method [30], hydrothermal method [31], liquid–solid-solution method [32], microemulsion-hydrothermal synthesis route [33,34], reverse micelle technique [35], template method [36], etc.), the semiconductor NCs synthesized by aqueous synthetic route have gained more research interest in recent years due to (i) high photoluminescence quantum yield [37], (ii) relatively narrow, symmetric luminescence bands [38], (iii) the superior tunability of the absorption over the very-broad spectral range [38], (iv) highly soluble in aqueous solutions [37], (v) as light emitters, can be compatible with water and the most-common biological buffers [39], and (vi) stable

* Corresponding author. Tel.: +86 028 85412415; fax: +86 028 85416050.
E-mail addresses: r.s.xie@163.com (R. Xie), nic0400@scu.edu.cn (J. Zhu).

0925-8388/$ – see front matter.
doi:10.1016/j.jallcom.2010.12.046

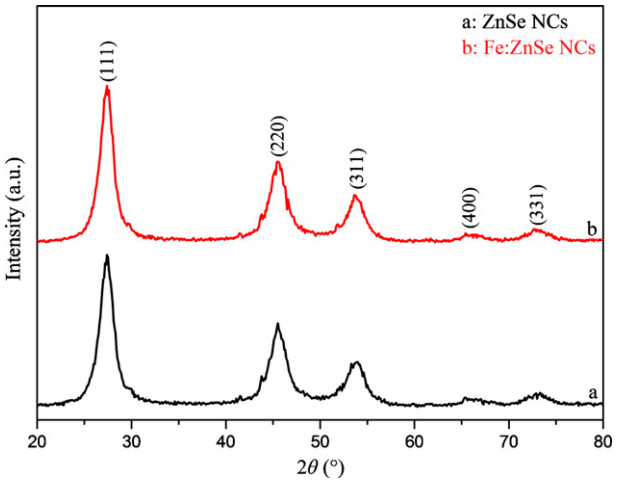

Fig. 1. XRD patterns of (a) undoped ZnSe and (b) Fe:ZnSe NCs.

in solution as well as solid phase [40], thus it can be stored for long periods.

To the best of our knowledge, literature on the Fe:ZnSe NCs have been scarcely reported. In present work, highly luminescent and water-soluble Fe:ZnSe NCs were prepared by aqueous synthesis approach. Surface capping and optical properties of the Fe:ZnSe semiconductor NCs were predominantly investigated, and the related physical mechanisms were also discussed.

2. Experimental procedures

Thioglycolic acid (TGA, $SHCH_2COOH$, 99%), selenium powder (Se, 99.9%), $Zn(CH_3COO)_2{\cdot}2H_2O$ (99.9%), $FeSO_4{\cdot}7H_2O$ (99.9%), and $NaBH_4$ (99.0%) were used as stating materials without further processing. The deionized water with a resistivity higher than 18 MΩ cm^{-1} was used in all experiments.

The Fe:ZnSe NCs were synthesized in aqueous solution under different conditions through the incorporation of iron ions into the ZnSe precursor NCs. All reactions were carried out in oxygen-free water under nitrogen protection. Sodium hydroselenide (NaHSe) was prepared by mixing sodium borohydride and selenium powder in water. In a typical experiment, 10 mL of freshly prepared NaHSe solution (0.02 M) was added into another solution containing $Zn(CH_3COO)_2{\cdot}2H_2O$ and TGA at a pH of 11 with vigorous stirring. The amounts of Zn, Se, and TGA introduced were controlled to be 0.198, 0.2, and 0.2574 mmol, respectively, in a total volume of 150 mL. The resulting mixture was heated to 130 °C, and the growth of TGA-capped ZnSe NCs began immediately. After heating at 130 °C for 2 h, 0.01–0.2 mL of 0.1 M of $FeSO_4{\cdot}7H_2O$ solution (0.001–0.02 mmol) pre-mixed with a slightly larger amount of TGA was added dropwise to the nanocrystalline ZnSe precursor solution. The as-prepared NCs were precipitated and washed several times by using 2-propanol, and then the purified NCs were dried at room temperature in vacuum overnight.

The phase structure of the obtained NCs was identified by using X-ray diffraction (XRD) (DX-1000, Dandong, China) with Cu Kα radiation. The grain sizes and morphology of the NCs were observed by transmission electron microscopy (TEM, JEM-2010, Shimadzu, Japan), where the TEM specimens were prepared by dispersing the NCs in deionized water and then dropping the NCs solution on a carbon film supported by a copper grid. Fourier-transform-infrared (FT-IR) spectrum of the NCs was recorded with a FT-IR spectrometer (Nicolet 6700, Thermo Scientific, USA). UV–Visible (UV–Vis) absorption spectra of the NCs were obtained using an UV–Visible spectrometer (UV-2100, Shimadzu, Japan). X-ray photoelectron spectroscopy (XPS) was carried out by using an X-ray photoelectron spectrometer (XSAM 800, Kratos, UK). The photoluminescence (PL) measurements were performed on a FL spectrophotometer (F-7000, Hatachi, Japan).

3. Results and discussion

Fig. 1 presents the XRD patterns of as-prepared undoped ZnSe and Fe:ZnSe NCs. The XRD peaks of all NCs can be indexed as the cubic zinc blende structure, which is consistent with the values in the Joint Committee on Powder Diffraction Standards (JCPDS) Card (File No. 80-0021). Moreover, the XRD patterns are broadened with three main peaks, which are corresponding to the (1 1 1), (2 2 0), and (3 1 1) planes, indicating the nanocrystalline nature of the samples.

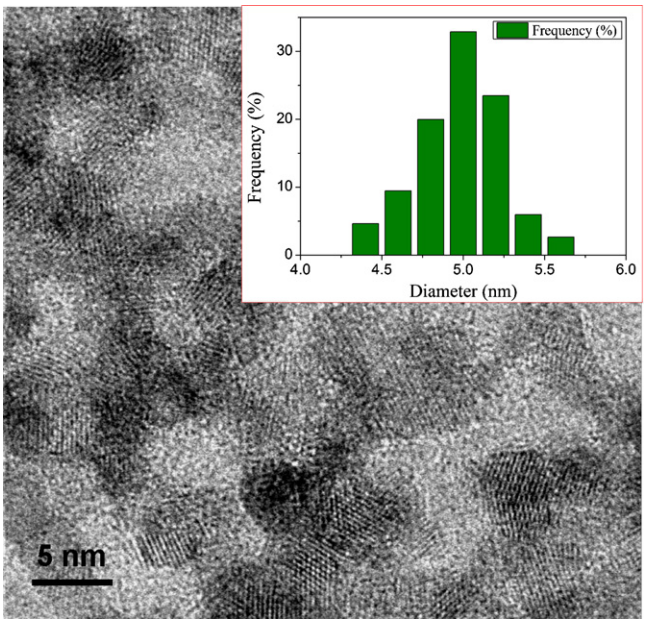

Fig. 2. TEM image of TGA-capped Fe:ZnSe NCs, the inset shows the corresponding size distribution diagram.

It is of interest to note that the introduction of Fe into ZnSe has not changed its zinc blende structure. In fact, no diffraction peaks corresponding to Fe precipitates or Fe-related impurity phase were detected, which further confirmed the formation of Fe:ZnSe solid solution instead of Fe precipitation or second phase, indicating that the Fe has been doped into the crystal lattice of ZnSe. Similar phenomenon was also observed for the Mn-doped CdSe reported by Oluwafemi et al. [41].

The mean crystallite size (D) was calculated according to the Scherrer formula [15] of $D = k\lambda/\beta\cos\theta$, where k is a constant (shape factor, about 0.9), λ is the X-ray wavelength (1.5405 Å, as mentioned before), β is the full width at half maximum (FWHM) of the diffraction line, and θ is the diffraction angle. Based on the FWHM of the reflection from (1 1 1) plane in zinc-blende structure, the average crystallite size of Fe:ZnSe NCs was estimated to be ~4.9 nm. It is worth mentioning that the calculated lattice constant (a) of pure ZnSe NCs, is ~0.5617 nm, which is the same as that from the JCPDS File No. 80-0021, $a = 0.5618$ nm. However, as for the Fe:ZnSe NCs ($a = 0.5615$), the lattice constant slightly decreases owing to the substitution of Fe^{2+} for Zn^{2+} because the diameter of Fe^{2+} (0.072 nm) is smaller than that of Zn^{2+} (0.074 nm) [42].

Fig. 2 demonstrates the typical TEM image and the corresponding size distribution diagram (the inset) of TGA-capped Fe:ZnSe NCs. The result shows that the as-synthesized Fe:ZnSe NCs are relatively uniform and approximately spherical in shape. The mean diameter is ~5 nm, which is in good agreement with the average particle size obtained using XRD results. The size distribution diagram further demonstrates the as-prepared Fe:ZnSe NCs have relatively narrow size distribution.

Fig. 3 displays the FT-IR spectrum of TGA-capped Fe:ZnSe NCs. The band at 3427 cm^{-1} corresponds to the –OH stretching [43], the peak at 1384 cm^{-1} is mainly due to C–OH stretching [43], and the band around 1623 cm^{-1} arises from the C=O stretching [43]. Both C–O stretching (1145 cm^{-1}) and C–S stretching (619 cm^{-1}) [43] are also detected from the FT-IR spectrum. In addition, no S–H bond stretching appears at 2568 cm^{-1} [43], which implies that the sulfhydryl (–SH) has bounded to Zn atoms to form a complex and the polar carboxylic acid group retains the surface of Fe:ZnSe NCs. This result indicates that TGA as the stabilizer capped the Fe:ZnSe NCs successfully.

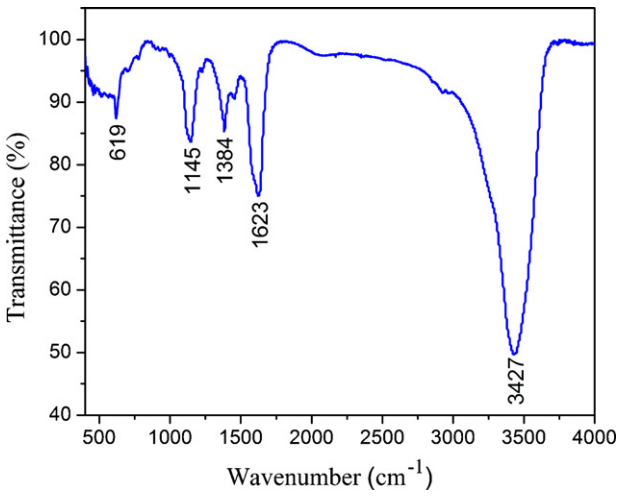

Fig. 3. FT-IR spectrum of TGA-capped Fe:ZnSe NCs.

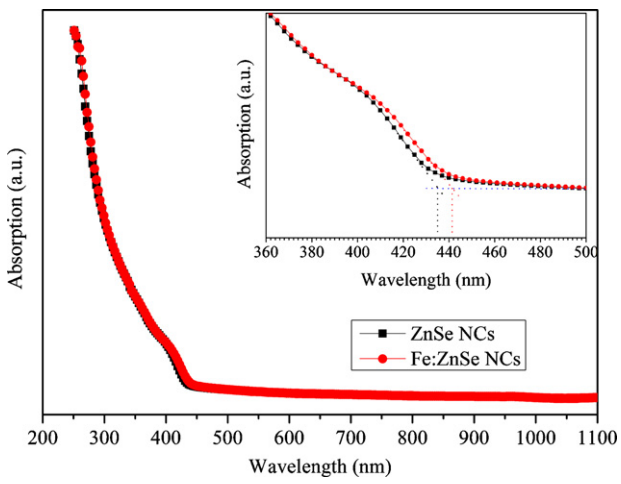

Fig. 4. UV–Vis absorption spectra of undoped ZnSe and Fe:ZnSe NCs.

The UV–Vis absorption spectra of pure ZnSe and Fe:ZnSe NCs are illustrated in Fig. 4. The absorption edge at ~435 nm is assigned to the characteristic absorption band edge of ZnSe NCs, which is blue-shifted as compared with the corresponding bulk band gap (2.69 eV) of ZnSe [16] due to quantum confinement effect. However, the absorption edge for the Fe:ZnSe NCs shows a slightly red shift with respect to the pure ZnSe NCs. Therefore, the incorporation of Fe ions in the ZnSe lattice does alter the absorption edge of the NCs significantly. Kumar and Singh [44] also observed similar red shift in Cu-doped ZnSe semiconductor quantum dots.

The properties of nanocrystalline materials show deviation from the corresponding bulk properties when the sizes of the crystallites become comparable to the Bohr excitonic radius. In this case, we observed the shift attributed to the spatial confinement of electron–hole pairs. Further, the blue shift of the band gap (ΔE_g) could also be utilized to determine the crystallite radius (r) using the effective mass approximation [45], given by:

$$\Delta E_g = E_g(r) - E_g(\text{bulk}) = \frac{\hbar^2\pi^2}{2r^2}\left(\frac{1}{m^*} + \frac{1}{m^*}\right) - \frac{1.8e^2}{4\pi\varepsilon\varepsilon_0 r} + S(r)$$

where $E_g(r)$ is the band gap energy of NCs, $E_g(\text{bulk}) = 2.69$ eV is the band gap energy of bulk ZnSe [16], m_e^* and m_h^* are the effective masses of the electron and hole in ZnSe ($m_e^* = 0.15\,m_0$, $m_h^* = 0.66\,m_0$, where $m_0 = 9.11 \times 10^{-28}$ g is the free-electron mass) [15], respectively; ε is the relative dielectric constant of the semiconductor ($\varepsilon = 9.1$) [46], ε_0 is the permittivity of vacuum, and r is the radius of NCs. $\hbar = 6.58 \times 10^{-16}$ eV is the reduced Plank constant, and $e = 1.6 \times 10^{-19}$ C is the electron charge. The last term $S(r)$, which is due to the spatial correlation between the electron and the hole, is generally small compared to the other terms and can be neglected. The band gap energy of NCs was estimated from the absorption coefficient data as a function of wavelength using Tauc's relation [47]: $(\alpha h\nu)^{1/n} = A(h\nu - E_g(r))$, where α is the absorption coefficient, $h\nu$ is the photon energy, A is a constant, $E_g(r)$ is the band gap energy of NCs, and n depends on type of transition ($n = 1/2$ for direct band gap and 2 for indirect band gap). For the Fe:ZnSe NCs sample, the particle diameter was estimated to be 4.7 nm from effective mass approximation, which matches well with the XRD results. Bulk Bohr exciton radius reported by Chin et al. [17] is 3.8 nm for the ZnSe. Therefore, our sample shows strong quantum confinement effect.

To further characterize the obtained Fe:ZnSe NCs, X-ray photoelectron spectroscopy (XPS) was carried out to investigate the surface composition and chemical state of Fe:ZnSe NCs, as plotted in Fig. 5. The detailed scan for Zn 2p spectrum comprises of two peaks with binding energies at 1022.0 eV and 1045.0 eV due to Zn $2p_{3/2}$ and Zn $2p_{1/2}$ [48], respectively. The detailed scan for Se 3d spectrum is also shown in Fig. 5, and the binding energy of Se 3d is 54.8 eV, and the peak is quite broad with full width at half maximum (FWHM) ~3.0 eV. It should be noted that the characteristic peak of Fe is not as strong as those of the other elements, which can be attributed to Fe being doped into the interior of particles. In addition, the binding energies of 709.2 and 722.9 eV correspond to the peaks of Fe $2p_{3/2}$ and Fe $2p_{1/2}$ [48], respectively, indicating that the Fe was successfully doped into the ZnSe NCs. Based on XPS results, we can deduce that the chemical reactions involved in the aqueous solution are as follows:

$$FeSO_4 + 2SHCH_2COOH + 2NaOH \rightarrow CH_2SCOOFe\downarrow + SHCH_2COOH + Na_2SO_4 + 2H_2O$$

$$CH_2SCOOFe + SHCH_2COOH + 2NaOH \rightarrow Fe(CH_2SCOONa)_2 + 2H_2O$$

$$4NaBH_4 + 2Se + 7H_2O \rightarrow 2NaHSe + Na_2B_4O_7 + 14H_2\uparrow$$

$$Zn(CH_3COO)_2 + NaHSe + SHCH_2COOH \xrightarrow{Fe(CH_2SCOONa)_2}$$

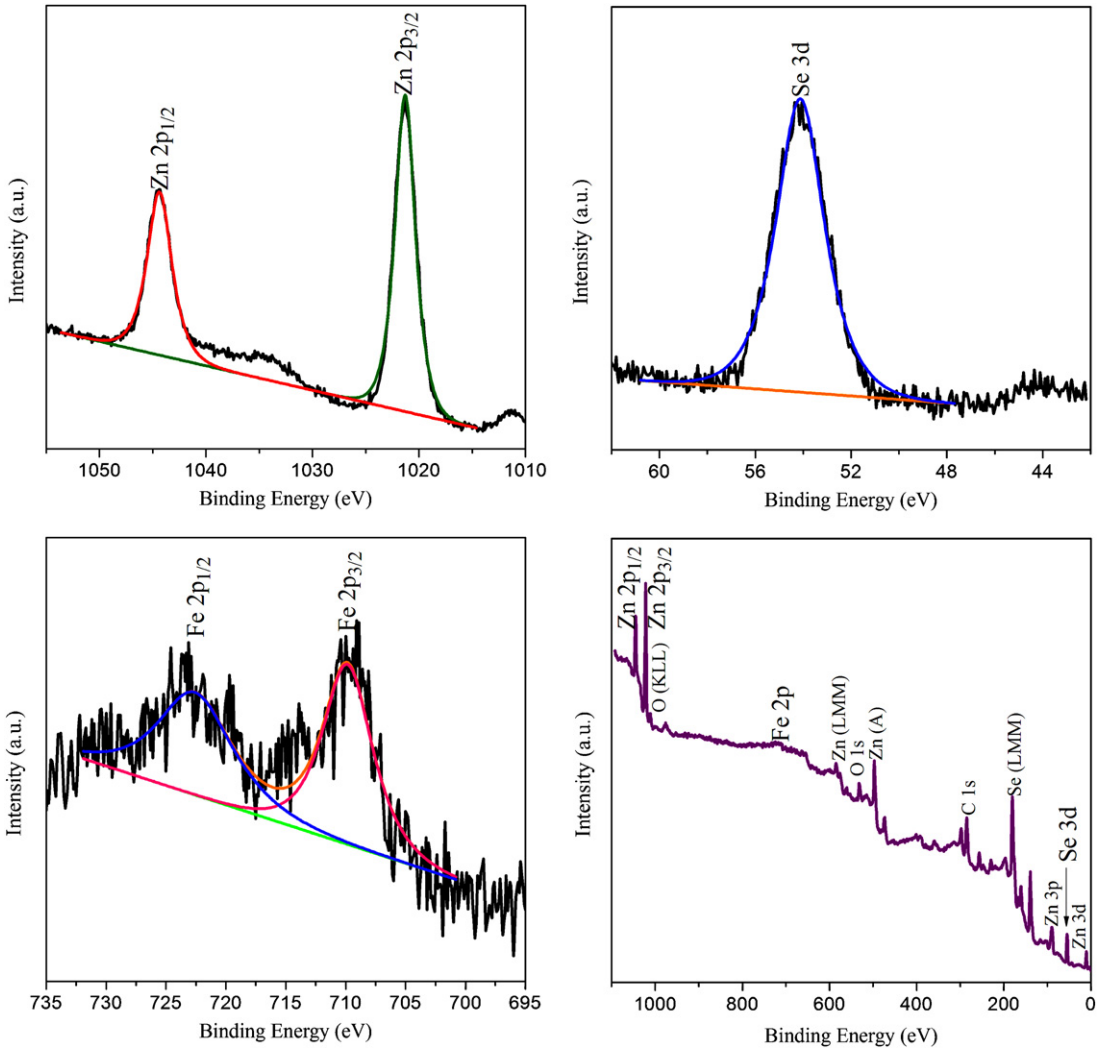

Fig. 5. X-ray photoelectron spectra of Fe:ZnSe NCs.

Fig. 6 exhibits the room-temperature PL spectra of as-prepared Fe:ZnSe NCs with different Fe-doping concentrations, showing an emission peak centered at around 425 nm under the excitation of 310 nm. The PL intensity of the NCs shows the maximum and minimum values when the Fe-doping concentration is 1.0 at% and 10.0 at%, respectively, indicating that the concentration quenching effect appears when the Fe doping concentration is larger than 10.0 at%. Many researchers have found the concentration quenching for the photoluminescence intensity of doped NCs. Cao et al. [49] observed the maximum luminescence at doping concentration of 3.0 at% in ZnS:Mn^{2+} nanoparticles. Klausch et al. [50] reported an optimal Cu^{2+} concentration of 0.5 mol% in ZnS:Cu nanoparticles. Unni et al. [51] found that the intensity decreases with increase of doping up to 6 wt%, increases for 6–10 wt% and then decreases and completely quenches at 15 wt% doping in CdS:Cu^{2+} quantum dots.

The mechanism of the PL process in Fe:ZnSe NCs is more or less well understood. Fe^{2+} ions occupy Zn^{2+} lattice sites in the ZnSe host lattice. In the PL process, an electron from the ZnSe valence band is excited across the band gap and the photo excited electron subsequently decays by a normal recombination process to some surface or defect states. At a higher Fe concentration, the isolated Fe ion may locate at the surface or interstitial positions of the crystallites with the octahedral symmetry, and these do not favor radiative transitions. As the Fe concentration in the doped NCs is more than 1.0 at%, Fe–Fe dipolar interactions may be predominant in the ZnSe host lat-

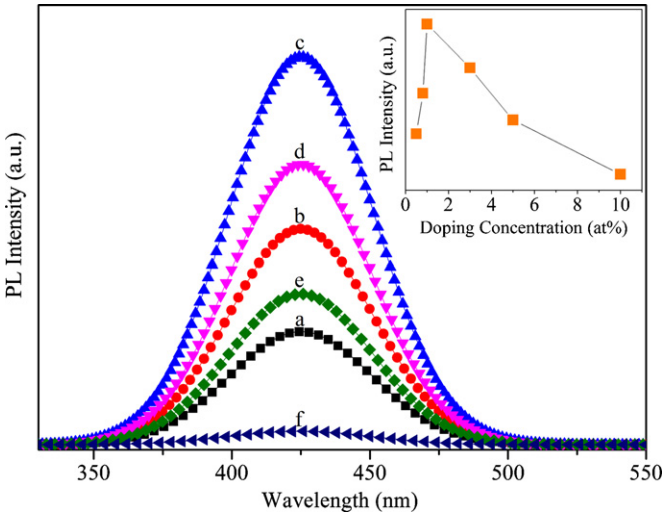

Fig. 6. PL spectra of Fe:ZnSe NCs with different Fe-doping concentrations (a) 0.5 at%, (b) 0.8 at%, (c) 1.0 at%, (d) 3.0 at%, (e) 5.0 at%, (f) 10.0 at%, the inset shows the variation in PL intensity with Fe-doping concentration.

tice. The emission intensity changes with different concentrations of Fe. This happens because not all the Fe^{2+} ions enter in the lattice in a substitutional manner at a higher concentration of Fe, but as explained above isolated Fe^{2+} ions may locate at the surface or interstitial positions. Therefore, although the luminescence intensity decreases due to the selenium vacancy, this is not accompanied by an increase of the Fe concentration.

4. Conclusions

Water-soluble TGA-capped Fe:ZnSe semiconductor NCs with zinc blende structure were successfully prepared by aqueous synthesis approach. The absorption edge of the Fe:ZnSe NCs is blue-shifted as compared with that of bulk ZnSe, indicating the quantum confinement effect. The PL intensity of the NCs shows the maximum value when the Fe-doping concentration is 1.0 at%, and the concentration quenching effect appears when the doping concentration is larger than 10.0 at%. Simple variations of this approach will enable direct synthesis of the NCs with a variety of compositions and properties.

Acknowledgment

This work was supported by the National Natural Science Foundation of China (60890203 and 60771016).

References

[1] Q.A. Zhang, J. Ding, Y.L. Shen, D.P. Chen, Q.L. Zhou, Q.X. Chen, Z.W. He, J.R. Qiu, J. Alloys Compd. 508 (2010) L13–L15.
[2] S. Wang, P. Li, H. Liu, J.B.A. Li, Y. Wei, J. Alloys Compd. 505 (2010) 362–366.
[3] M. Salavati-Niasari, A. Sobhani, F. Davar, J. Alloys Compd. 507 (2010) 77–83.
[4] M. Romcevic, N. Romcevic, R. Kostic, L. Klopotowski, W.D. Dobrowolski, J. Kossut, M.I. Comor, J. Alloys Compd. 497 (2010) 46–51.
[5] J. Li, X.S. Tang, Z.Y. Lu, Y.T. Qian, J. Alloys Compd. 497 (2010) 390–395.
[6] P.V. Jyothy, K.V.A. Kumar, S. Karthika, R. Rajesh, N.V. Unnikrishnan, J. Alloys Compd. 493 (2010) 223–226.
[7] B.H. Dong, L.X. Cao, G. Su, W. Liu, H. Qu, H. Zhai, J. Alloys Compd. 492 (2010) 363–367.
[8] Z.G. Chen, Q.W. Tian, Y.L. Song, J.M. Yang, J.Q. Hu, J. Alloys Compd. 506 (2010) 804–810.
[9] C.H. Lu, B. Bhattacharjee, S.Y. Chen, J. Alloys Compd. 475 (2009) 116–121.
[10] F. Li, W.T. Bi, T. Kong, C.J. Wang, Z. Li, X.T. Huang, J. Alloys Compd. 479 (2009) 707–710.
[11] D.V. Talapin, J.S. Lee, M.V. Kovalenko, E.V. Shevchenko, Chem. Rev. 110 (2010) 389–458.
[12] V. Biju, T. Itoh, M. Ishikawa, Chem. Soc. Rev. 39 (2010) 3031–3056.
[13] N. Pradhan, X.G. Peng, J. Am. Chem. Soc. 129 (2007) 3339–3347.
[14] N.S. Norberg, G.L. Parks, G.M. Salley, D.R. Gamelin, J. Am. Chem. Soc. 128 (2006) 13195–13203.
[15] S.M. Emin, N. Sogoshi, S. Nakabayashi, T. Fujihara, C.D. Dushkin, J. Phys. Chem. C 113 (2009) 3998–4007.
[16] X.D. Liu, J.M. Ma, P. Peng, W.J. Meng, Langmuir 26 (2010) 9968–9973.
[17] P.T.K. Chin, J.W. Stouwdam, R.A.J. Janssen, Nano Lett. 9 (2009) 745–750.
[18] Y.P. Leung, W.C.H. Choy, I. Markov, G.K.H. Pang, H.C. Ong, T.I. Yuk, Appl. Phys. Lett. 88 (2006) 183110.
[19] C.H. Hsiao, S.J. Chang, S.B. Wang, S.C. Hung, S.P. Chang, T.C. Li, W.J. Lin, B.R. Huang, Superlattices Microst. 46 (2009) 572–577.
[20] B. Goswami, S. Pal, C. Ghosh, P. Sarkar, J. Phys. Chem. C 113 (2009) 6439–6443.
[21] H.T. Wang, T. Tian, S.C. Yan, N.P. Huang, Z.D. Xiao, J. Cryst. Growth 311 (2009) 3787–3791.
[22] S.A. Santangelo, E.A. Hinds, V.A. Vlaskin, P.I. Archer, D.R. Gamelin, J. Am. Chem. Soc. 129 (2007) 3973–3978.
[23] N. Pradhan, D. Goorskey, J. Thessing, X.G. Peng, J. Am. Chem. Soc. 127 (2005) 17586–17587.
[24] H.B. Shen, H.Z. Wang, X.M. Li, J.Z. Niu, H. Wang, X. Chen, L.S. Li, Dalton Trans. (2009) 10534–10540.
[25] S. Jana, B.B. Srivastava, S. Acharya, P.K. Santra, N.R. Jana, D.D. Sarma, N. Pradhan, Chem. Commun. 46 (2010) 2853–2855.
[26] D.A. Chen, R. Viswanatha, G.L. Ong, R.G. Xie, M. Balasubramaninan, X.G. Peng, J. Am. Chem. Soc. 131 (2009) 9333–9339.
[27] S. Acharya, D.D. Sarma, N.R. Jana, N. Pradhan, J. Phys. Chem. Lett. 1 (2010) 485–488.
[28] L.J. Zu, D.J. Norris, T.A. Kennedy, S.C. Erwin, A.L. Efros, Nano Lett. 6 (2006) 334–340.
[29] R.S. Zeng, M. Rutherford, R.G. Xie, B.S. Zou, X.G. Peng, Chem. Mat. 22 (2010) 2107–2113.
[30] B. Tripathi, Y.K. Vijay, S. Wate, F. Singh, D.K. Avasthi, Solid-State Electron. 51 (2007) 81–84.
[31] Z.Y. Ren, H. Yang, L.C. Shen, S.D. Han, J. Mater. Sci.: Mater. Electron. 19 (2008) 1–4.
[32] D.R. Jung, D. Son, J. Kim, C. Kim, B. Park, Appl. Phys. Lett. 93 (2008) 163118.
[33] F.H. Su, Z.L. Fang, B.S. Ma, K. Ding, G.H. Li, S.J. Xu, J. Appl. Phys. 95 (2004) 3344–3349.
[34] J. Liu, J.F. Ma, Y. Liu, Z.W. Song, Y. Sun, J.R. Fang, Z.S. Liu, J. Alloys Compd. 486 (2009) L40–L43.
[35] Y.M. Sung, W.C. Kwak, T.G. Kim, Cryst. Growth Des. 8 (2008) 1186–1190.
[36] A.D. Dinsmore, D.S. Hsu, S.B. Qadri, J.O. Cross, T.A. Kennedy, H.F. Gray, B.R. Ratna, J. Appl. Phys. 88 (2000) 4985–4993.
[37] A.L. Rogach, T. Franzl, T.A. Klar, J. Feldmann, N. Gaponik, V. Lesnyak, A. Shavel, A. Eychmuller, Y.P. Rakovich, J.F. Donegan, J. Phys. Chem. C 111 (2007) 14628–14637.
[38] N. Gaponik, S.G. Hickey, D. Dorfs, A.L. Rogach, A. Eychmuller, Small 6 (2010) 1364–1378.
[39] K. Boldt, O.T. Bruns, N. Gaponik, A. Eychmuller, J. Phys. Chem. B 110 (2006) 1959–1963.
[40] S. Jagadeeswari, M. Asha Jhonsi, A. Kathiravan, R. Renganathan, J. Lumin. (2010), doi:10.1016/j.jlumin.2010.10.037.
[41] O.S. Oluwafemi, N. Revaprasadu, O.O. Adeyemi, Mater. Lett. 64 (2010) 1513–1516.
[42] R. Shannon, Acta Crystallogr. Sect. A 32 (1976) 751–767.
[43] B.D. Mistry, Handbook of Spectroscopic Data: Chemistry – UV, IR, PMR, CNMR and Mass Spectroscopy, 2009 ed., Oxford Book Company, Jaipur, 2009.
[44] P. Kumar, K. Singh, J. Nanopart. Res. (2010), doi:10.1007/s11051-11010-19914-11055.
[45] L.E. Brus, J. Chem. Phys. 80 (1984) 4403–4409.
[46] B.C. Mei, J. Wang, Q. Qiu, T. Heckler, A. Petrou, T.J. Mountziaris, Appl. Phys. Lett. 93 (2008) 083114.
[47] J. Tauc, A. Menth, J. Non-Cryst. Solids 8–10 (1972) 569–585.
[48] J.F. Moulder, W.F. Stickle, P.E. Sobol, K.D. Bomben, Handbook of X-Ray Photoelectron Spectroscopy, 1st ed., Perkin-Elmer Corporation, Minnesota, 1979.
[49] J. Cao, J.H. Yang, Y.J. Zhang, L.L. Yang, Y.X. Wang, M.B. Wei, Y. Liu, M. Gao, X.Y. Liu, Z. Xie, J. Alloys Compd. 486 (2009) 890–894.
[50] A. Klausch, H. Althues, C. Schrage, P. Simon, A. Szatkowski, M. Bredol, D. Adam, S. Kaskel, J. Lumin. 130 (2010) 692–697.
[51] C. Unni, D. Philip, S.L. Smitha, K.M. Nissamudeen, K.G. Gopchandran, Spectrochim. Acta A: Mol. Biomol. Spectrosc. 72 (2009) 827–832.